AGU PUBLICATIONS

Geophysical Research Letters

RESEARCH LETTER
10.1002/2014GL062522

Key Points:
- Ocean warming increases internal wave activity in the South China Sea
- El Niño and the Kuroshio Current drive interannual internal wave variability
- Internal wave activity is projected to increase in the 21st century

Correspondence to:
T. M. DeCarlo,
tdecarlo@whoi.edu

Citation:
DeCarlo, T. M., K. B. Karnauskas, K. A. Davis, and G. T. F. Wong (2015), Climate modulates internal wave activity in the Northern South China Sea, *Geophys. Res. Lett.*, *42*, doi:10.1002/2014GL062522.

Received 13 NOV 2014
Accepted 15 JAN 2015
Accepted article online 19 JAN 2015

Climate modulates internal wave activity in the Northern South China Sea

Thomas M. DeCarlo[1], Kristopher B. Karnauskas[2], Kristen A. Davis[3], and George T. F. Wong[4]

[1]Massachusetts Institute of Technology/Woods Hole Oceanographic Institution Joint Program in Oceanography/Applied Ocean Physics and Engineering, and Department of Geology and Geophysics, Woods Hole Oceanographic Institution, Woods Hole, Massachusetts, USA, [2]Woods Hole Oceanographic Institution, Woods Hole, Massachusetts, USA, [3]Civil and Environmental Engineering, University of California, Irvine, California, USA, [4]Research Center for Environmental Changes, Academia Sinica, Taipei, Taiwan

Abstract Internal waves (IWs) generated in the Luzon Strait propagate into the Northern South China Sea (NSCS), enhancing biological productivity and affecting coral reefs by modulating nutrient concentrations and temperature. Here we use a state-of-the-art ocean data assimilation system to reconstruct water column stratification in the Luzon Strait as a proxy for IW activity in the NSCS and diagnose mechanisms for its variability. Interannual variability of stratification is driven by intrusions of the Kuroshio Current into the Luzon Strait and freshwater fluxes associated with the El Niño–Southern Oscillation. Warming in the upper 100 m of the ocean caused a trend of increasing IW activity since 1900, consistent with global climate model experiments that show stratification in the Luzon Strait increases in response to radiative forcing. IW activity is expected to increase in the NSCS through the 21st century, with implications for mitigating climate change impacts on coastal ecosystems.

1. Introduction

Internal waves (IWs)—waves propagating along density gradients within a fluid—are ubiquitous features throughout the world ocean [*Nash et al.*, 2012a]. Sharp vertical density gradients exist between different water masses within the ocean, most notably across the pycnocline, a steep vertical density gradient usually located in the upper several hundred meters of the water column. Perturbations to such a density gradient are restored by buoyancy, generating a propagating wave. Globally, IWs play an important role in diapycnal mixing [*Gregg et al.*, 2003], delivering nutrients to the surface ocean that stimulate phytoplankton growth [*Holligan et al.*, 1985]. The amplitude and presence/absence of IWs vary among coastal regions of the world, due in part to spatial variability in remote IW generation, propagation, and local topography, and also due to changes in local stratification and circulation [*Nash et al.*, 2012a]. In certain locations, such as the Luzon Strait in the Northern South China Sea (NSCS), where strong vertical density gradients interact with shallow bottom topography, IWs are persistent and dominant features of the regional ocean climate [e.g., *Ramp et al.*, 2010; *Fu et al.*, 2012].

Some of the ocean's largest IWs occur within the NSCS [*Ramp et al.*, 2010; *Fu et al.*, 2012]. The surface tide, or barotropic tide, moves a stratified water column across two shallow ridges in the Luzon Strait between Taiwan and the Philippines [*Ramp et al.*, 2010], generating IWs. The IWs generated in the Luzon Strait begin as westward propagating depression waves, where shallow water is brought to depth, and transition to elevation waves, where deep water is brought toward the surface, as they interact with shallow topography [*Fu et al.*, 2012]. On their path across the NSCS, the IWs collide directly with Dongsha Atoll [*Fu et al.*, 2012] (Figure 1), where fore reef coral communities experience cool temperature anomalies and primary productivity is stimulated [*Wang et al.*, 2007; *Pan et al.*, 2012]. Corals living on Dongsha may benefit from exposure to cooler, nutrient-rich water delivered by IWs for several reasons. First, laboratory culture experiments show that elevated nutrient concentrations reduce the sensitivity of coral calcification to ocean acidification [e.g., *Holcomb et al.*, 2010]. IWs likely elevate plankton flux onto the reef and increase coral heterotrophy, as has been shown where IWs interact with coral reefs in the Andaman Sea [*Roder et al.*, 2010]. In laboratory experiments, heterotrophy has been shown to enhance coral biomass and calcification [*Edmunds*, 2011; *Drenkard et al.*, 2013]. Further, IWs may provide thermal relief in the form of cooler water to corals in periods of otherwise anomalously warm sea surface temperature (SST) [*Wall et al.*, 2015]. For example, corals living at 5–7 m depth in the Dongsha lagoon that are relatively isolated from IWs bleached during the 1998 high-temperature anomaly with almost complete mortality, while corals at similar depths on the fore reef, where IWs are active (Figure 1), did not bleach [*Dai*, 2004].

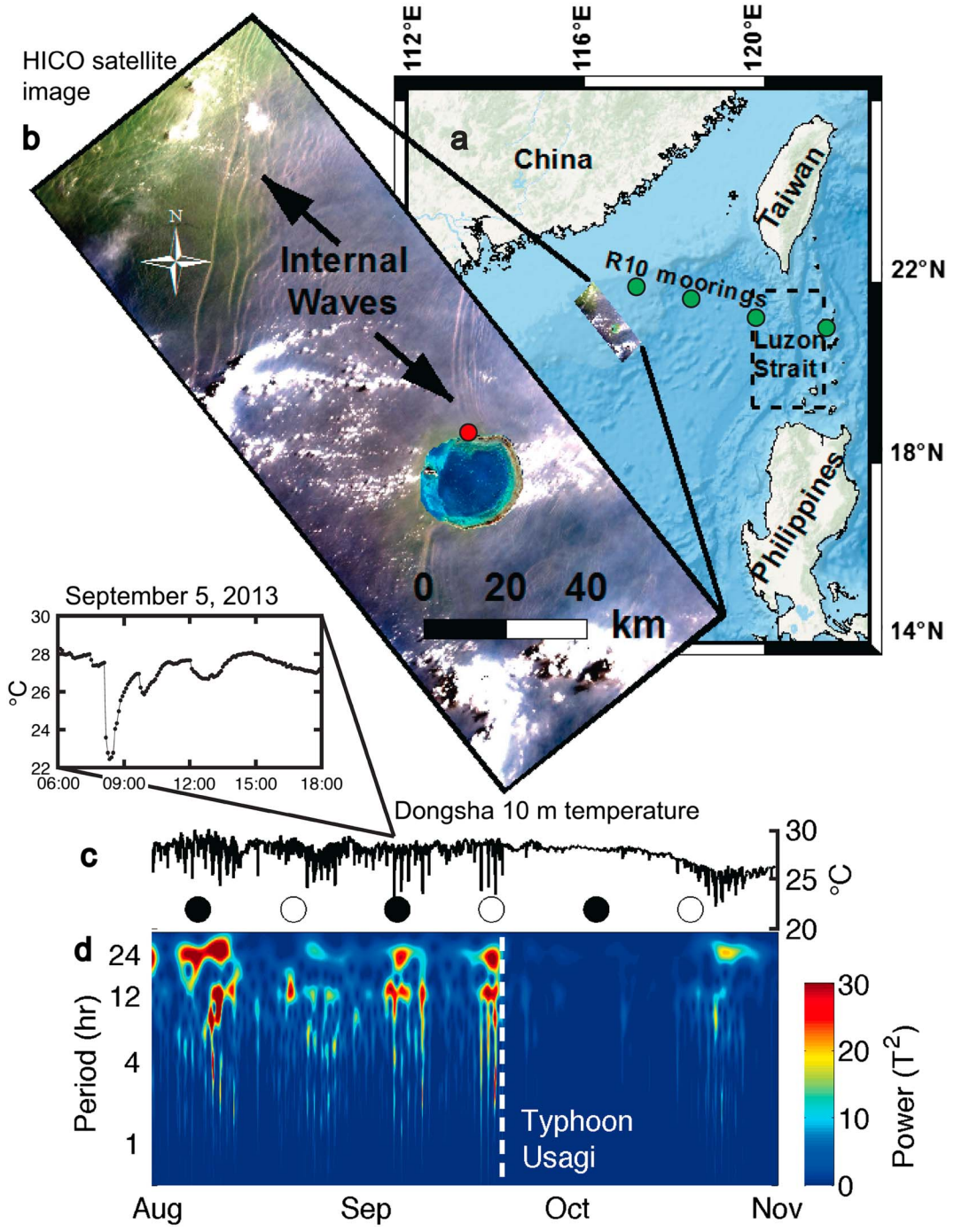

Figure 1. Internal waves in the Northern South China Sea. (a) Map of the NSCS indicating the locations of the Luzon Strait domain (dashed box) and the *Ramp et al.* [2010] moorings (labeled "R10" and plotted as green dots). (b) IWs are visible around Dongsha Atoll in a satellite image taken on 28 May 2014 by the Hyperspectral Imager for the Coastal Ocean (HICO). (c) Temperature recorded at 10 m depth shows IW activity on the Dongsha fore reef (red dot in HICO image) from August through October 2013, and zoom in to show a typical IW packet observed on 5 September 2013. Filled and open circles indicate the lunar phases corresponding to spring tides, when IW activity was greatest. (d) Internal waves appear as pulses of high variance (red colors) distributed between ~2 and 24 h periods in a wavelet power spectrum. The vertical dashed white line indicates when Typhoon Usagi passed through Luzon Strait, which marks the beginning of a period of IW quiescence.

2. Stratification and Internal Waves

The background oceanic density field has both spatial and temporal variability, which can affect IW generation and propagation. To understand the effects of stratification on IW dynamics, we consider the equation governing baroclinic flow in perturbation form, as in *Baines* [1982]

$$\frac{\partial \mathbf{u}_{bc}}{\partial t} + f \times \mathbf{u}_{bc} + \frac{1}{\overline{\rho_0}} \nabla p_{bc} + \frac{\rho_{bc} g}{\overline{\rho_0}} \hat{\mathbf{z}} = F_B = -\frac{g \rho_{bt}}{\overline{\rho_0}} \hat{\mathbf{z}} \tag{1}$$

where $\mathbf{u}_{bc}$ and p_{bc} are the baroclinic components of the velocity and pressure fields, respectively, the density field is decomposed into the background density (ρ_0) and the density perturbations caused by barotropic (ρ_{bt}) and baroclinic (ρ_{bc}) motions, f is the Coriolis frequency, t is time, g is gravitational acceleration, and $\hat{\mathbf{z}}$ is the unit vector in the upward direction. F_B is often called the "Baines force" and is a linear forcing term that represents the generation of IWs from vertical density perturbations due to barotropic tidal motions. Defining ρ_{bt} in terms of the background density gradient and the vertical, barotropic velocity component, w_{bt}, the Baines force becomes

$$F_B = \left(-\frac{g}{\overline{\rho_0}} \frac{\partial \rho_0}{\partial z} \right) w_{bt} \omega_{bt}^{-1} = N^2 w_{bt} \omega_{bt}^{-1} \tag{2}$$

where ω_{bt} is the barotropic tidal frequency and N is the Brunt-Väisälä buoyancy frequency

$$N = \sqrt{\frac{-g}{\overline{\rho_0}} \frac{\partial \rho_0}{\partial z}} \tag{3}$$

The form of the Baines force term in equation (2) illustrates that the conversion of barotropic tidal energy to baroclinic motions (i.e., IWs) is proportional to N^2. Consistent with this theory, models of IW generation, including 3-D numerical simulations of IW generation over the topography of the Luzon Strait, show that increasing stratification increases IW generation by the barotropic tide [*Chuang and Wang*, 1981; *Zheng et al*., 2007; *Shaw et al*., 2009; *Zhang et al*., 2011].

Perturbations within different density stratification fields can produce waves which differ in their frequency and propagation angle according to the IW dispersion relation, $\omega_{iw}{}^2 = N^2 cos^2\theta + f^2 sin^2\theta$, where ω_{iw} is the IW frequency, and θ is the angle of the IW characteristic [*Phillips*, 1977]. Thus, changes in N can modify the angle at which IWs propagate once generated. A strong, shallow (within the upper ~100 m) pycnocline, like that characteristic of the NSCS [*Zhao and Alford*, 2006], is critical in that it acts as a waveguide, concentrating the IW energy near the surface [*Shaw et al*., 2009], and ultimately increases the transmission of IW energy onto shallow shelves. For example, numerical experiments performed with two different stratifications using a 2-D model of the New Jersey continental shelf show that a 25% increase in N^2 produces a 50% increase in the flux of IW energy onto the shelf [*Nash et al*., 2012b]. Consistent with this theory, observations of IWs by moored current profilers show that greater stratification in the Luzon Strait leads to greater IW energy flux onto the continental slope in the NSCS [*Ma et al*., 2013].

The theoretical link between stratification and IW generation is consistent with the longest continuous observations of IWs in the NSCS from May 2005 through May 2006 via temperature, velocity, and pressure measurements on four moorings spanning the NSCS basin to the upper continental slope westward of the Luzon Strait [*Ramp et al*., 2010]. These previous direct observations revealed the diurnal arrival of IW packets that occurred generally within ±4 days of spring tide from the start of observation in May 2005, almost completely ceased between December 2005 and March 2006, and resumed in April 2006 [*Ramp et al*., 2010]. This seasonal pattern of IW presence (absence) is explained by high (low) stratification in the Luzon Strait measured from conductivity-temperature-depth casts [*Ramp et al*., 2010], consistent with IW generation observed elsewhere around the world [*Nash et al*., 2012a]. The few IWs that were formed during winter 2005 and 2006 occurred only during anomalous high-stratification events [*Ramp et al*., 2010].

Past and future changes in IW activity likely play an important role in the ecology of Dongsha Atoll and other marine ecosystems in the NSCS. Yet we are aware of no study that has documented IW activity in the NSCS on decadal or longer time scales. Here we use the Simple Ocean Data Assimilation (SODA) system, version 2.2.4, an ocean model constrained by in situ observations [*Carton and Giese*, 2008; *Giese*

and Ray, 2011] to reconstruct historical changes since 1900 in stratification (N) in the Luzon Strait, which serves as an indirect measure of IW activity based on the theory and observations discussed above, combined with our own unique observations of IW activity on Dongsha Atoll presented here.

3. Methods

We characterized IW activity at Dongsha Atoll via a time series of temperature, which tracks oscillations of the thermocline driven by IWs. Temperature at 10 m depth on the Dongsha Atoll northern fore reef was measured at a 5 min sampling interval from August through October 2013 with an Onset Corporation HOBO U22 logger (accuracy ± 0.1°C after calibration in an isothermal bath) attached to a buoy 1 m above the bed. In order to identify the IW signal, we applied a continuous wavelet transform to the temperature time series following the methods described by *Torrence and Compo* [1998], using a Morlet wavelet. IWs appear in the wavelet power spectrum as bursts of power that are distributed across periods (Figure 1); the reason for this is shown by the arrival of a typical IW packet that occurred on 5 September 2013 (Figure 1). Temperature was depressed from ~08:00 to ~13:00, casting power onto low frequencies (10+ h periods). Superimposed on this 5 h anomaly are higher-frequency cool anomalies that occur over 1-2 h. Thus, the approximately daily pulses of power distributed across periods in the wavelet power spectrum indicate the arrival of these IW packets.

To characterize historical IW activity in the NSCS, we analyzed the density stratification, as N (equation (3)), in the Luzon Strait (19–21.5°N, 120–121.5°E) in the SODA reanalysis from 1900 to 2008. We excluded the nineteenth century SODA reanalysis (beginning in 1871) because of its reliance upon atmospheric data and sparse SST observations rather than hydrographic depth profiles [*Giese and Ray*, 2011]. N was calculated in each grid box from vertical profiles of temperature and salinity in SODA using the Gibbs Seawater Toolbox [*McDougall*, 2011]. Stratification data were reduced to a one-dimensional monthly time series of maximum N by first finding the maximum N in the vertical profile below each surface grid box within the Luzon Strait and then taking the mean of all maximum N grid points at each month ($n = 15$ grid boxes); this monthly time series was then averaged into seasonal and annual time series. Throughout the text, "N" refers to these time series of N maxima with respect to depth.

The separate influence of temperature and salinity on Luzon Strait N can be evaluated by holding one variable to a climatological mean, while using the historical reanalysis of the other variable. To do this, we repeated our analysis of SODA using the climatological monthly mean temperature and salinity depth profiles, separately (i.e., variability of N becomes a function of only temperature or salinity variability).

More than 99% of monthly N maxima were found within the upper 125 m in SODA, consistent with the depths where IWs are observed [*Ramp et al*., 2010], and where the strong pycnocline is modeled to act as a waveguide [*Shaw et al*., 2009], within the NSCS. We also used sea surface height (SSH) anomalies in SODA to identify the location of the Kuroshio Current. SODA has been shown to reliably reproduce both interannual variability of Kuroshio transport [*Wu et al*., 2012] and SSH in the South China Sea [*Yang and Wu*, 2012], supporting the ability of SODA to constrain Kuroshio intrusions in the Luzon Strait.

We used ordinary least squares linear regression to test for significant ($p < 0.05$) trends of N with respect to time for both the seasonal and annual time series. Because the time series are significantly autocorrelated at a lag of 1 year, we test for significance with a reduced effective number of degrees of freedom ($n_{\text{effective}} = n(1 - r)/(1 + r)$, where r is the lag 1 autocorrelation coefficient of the detrended series). In addition, we used ordinary least squares to test for significant correlations between annual Luzon Strait N and the following time series: the NINO3.4 index of El Niño–Southern Oscillation (ENSO) [*Trenberth and Stepaniak*, 2001], SST from the NOAA Extended Reconstructed SST (ERSST.v3b) data set [*Smith et al*., 2008], and mean SSH in the Luzon Strait from SODA.

Using the same procedure as for SODA, we analyzed Luzon Strait N within the National Center for Atmospheric Research (NCAR) Community Climate System Model version 4 (CCSM4) coupled general circulation model (GCM) (12 grid points in the Luzon Strait) ensemble member r1i1p1 (this code identifies which initial conditions were selected from a set of equally likely initial conditions). The historical CCSM4 simulation has radiative forcing consistent with historical greenhouse gas emissions, but such simulations are not constrained to match the timing of observed interannual climate variability. Therefore, we only compare the centennial-scale trends between CCSM4 and SODA because it is the trend that represents the

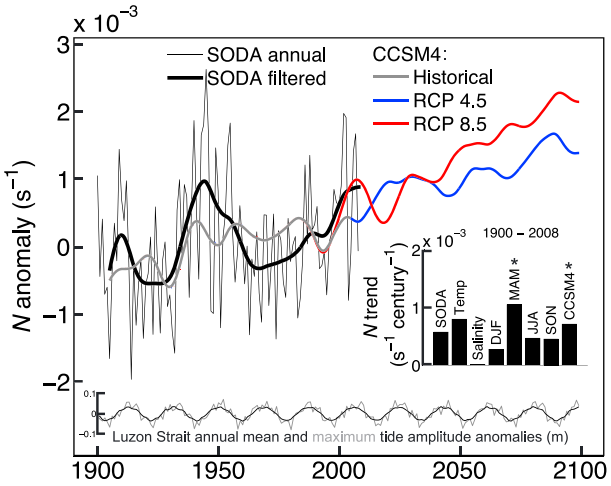

Figure 2. Temporal changes in Luzon Strait stratification. Time series of Luzon Strait annual (thin black) and 20 year low-pass filtered (thick black) *N* anomalies relative to the 1900–2000 mean derived from SODA, and historical (gray), RCP 4.5 (blue), and RCP 8.5 (red) *N* anomalies derived from CCSM4. Inset bar plot shows linear trends of historical *N* changes derived from temperature and salinity together (SODA), temperature alone (Temp), salinity alone (Salinity), seasonal changes in temperature and salinity in SODA, and CCSM4. Seasons are defined such that winter is December-January-February (DJF), spring is March-April-May (MAM), summer is June-July-August (JJA), and autumn is September-October-November (SON). Asterisks indicate significant trends after correcting the effective degrees of freedom for autocorrelation (see methods). From 1958 to 2008, when SODA is constrained by comprehensive hydrographic observations [*Giese and Ray*, 2011], the linear trend of *N* is significant ($2.3 \pm 1.6 \times 10^{-3}$ s^{-1} century^{-1}). Inset time series shows annual mean (black) and maximum (gray) tidal amplitude (in meters) in the Luzon Strait calculated for each year from the range of sea level within 2 day windows. The plot shows anomalies relative to 1900–2100 means, with mean annual amplitude of 0.71 m and mean of annual maximum amplitude of 1.10 m.

response to historical radiative forcing. We predicted Luzon Strait *N* throughout the 21st century using CCSM4 simulations under different greenhouse gas emission scenarios, which are called "representative concentration pathways" (RCPs), that correspond to "high" (RCP8.5) and "midrange mitigation" (RCP4.5) emission scenarios [*Taylor et al.*, 2012].

4. Results and Discussion

4.1. Internal Waves at Dongsha Atoll

Our time series of IW activity at Dongsha Atoll follows the pattern of IW generation in the Luzon Strait. IWs on Dongsha generate cold temperature anomalies up to 6°C and have a fortnightly beat, with the greatest IW activity generally occurring 2 days after the spring tide (Figure 1), consistent with the timing of IWs generated in the Luzon Strait and 2 days for the IWs to propagate to Dongsha [*Ramp et al.*, 2010]. Typhoon Usagi passed directly through the Luzon Strait on 21 September 2013, presumably increasing the mixed layer depth and decreasing stratification, as shown following previous typhoons near the Luzon Strait [*Lin et al.*, 2003]. Immediately following Typhoon Usagi, IW activity ceased at Dongsha for 1 month (Figure 1). These data are consistent with the theory and previous observations described in section 2, and further underscore the critical dependence of IWs at the Dongsha coral reef, and likely throughout the NSCS, on Luzon Strait stratification. The lack of IWs at 10 m depth on the Dongsha fore reef is potentially explained by smaller amplitude or deeper IWs following Usagi. Nevertheless, it is clear that the extent to which the shallow coral reef ecosystem on Dongsha is exposed to IWs is sensitive to changes in the water column between Luzon Strait and Dongsha.

4.2. Roles of Ocean Warming, ENSO, and the Kuroshio in Modulating Internal Waves

Annual and seasonal *N* in the Luzon Strait have increased since 1900 (Figure 2), implying an increase in IW activity in the NSCS. Increasing stratification in the Luzon Strait arises dominantly from temperature changes in the upper 100 m. Calculating the annual *N* time series using climatological monthly mean salinity (only temperature varying) captures 69% of the total variance and a similar trend as the full analysis (Figure 2), while changing salinity alone captures only 35% of total variance and produces no long-term trend of *N* since 1900. The relative contributions of temperature and salinity changes to the Luzon Strait *N* trend are further evaluated by comparing temporal changes of density depth gradients due to changes in temperature and salinity (Figure 3). Seasonal-depth patterns of *N* change, in particular the increasing *N* at the depths of climatological maximum stratification, are nearly replicated by the density depth-gradient changes attributable to temperature, with little contribution from changing salinity. Together, these results clearly show that it is warming in the surface ocean that is responsible for the trend of increasing stratification in the Luzon Strait over the past century.

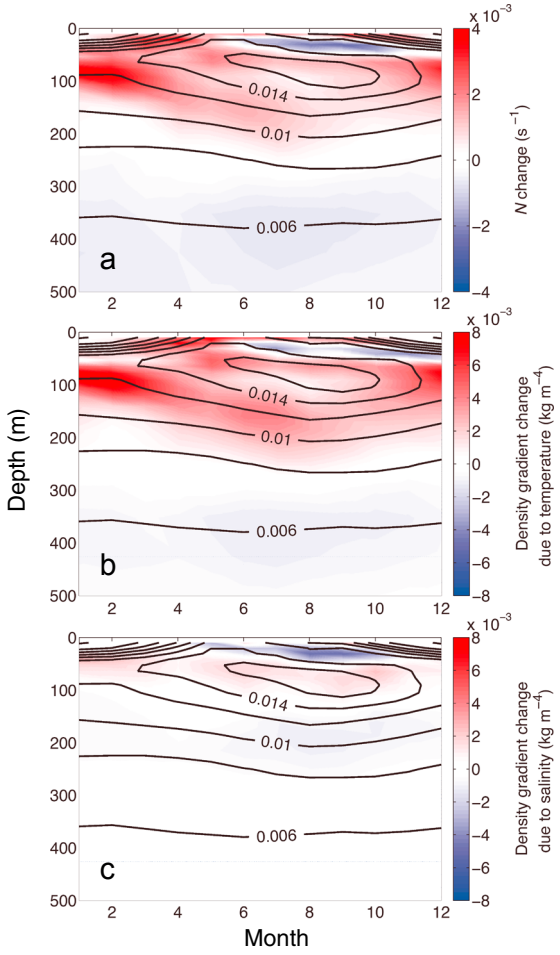

Figure 3. Seasonal and depth patterns of stratification changes in the Luzon Strait. (a) Difference in Luzon Strait *N*, (b) vertical temperature gradient, and (c) vertical salinity gradient between 1983–2008 and 1900–1925 (colors) as functions of depth and month. Change in temperature and salinity depth gradients is converted to change in density depth gradient at 34.5 practical salinity unit and 25°C, respectively. The climatological monthly mean buoyancy frequency is shown by the contours. Contour spacing is 0.002 s^{-1}.

Interannual variability is superimposed on the long-term trend of stratification in the Luzon Strait. Some of this interannual variability is related to the Pacific basin pattern of ENSO. Detrended annual Luzon Strait *N* is significantly inversely correlated with the NINO3.4 index. In general, anomalously high stratification occurs in the Luzon Strait during La Niña, and anomalously low stratification during El Niño. To understand how ENSO influences Luzon Strait *N*, we compare the correlation with ENSO using the SODA analyses of Luzon Strait *N* with climatological mean temperature and salinity, separately (Figure 4). This shows that the ENSO-like pattern dominates the spatial correlation between tropical SST and annual Luzon Strait *N* calculated with climatological mean temperature (salinity varying) but is largely absent in the analysis repeated with climatological mean salinity (Figure 4). Because the connection to ENSO is driven by salinity variations (rather than temperature) in the Luzon Strait, this pattern can be explained if La Niña causes (1) an absence of salty Kuroshio Current intrusions or (2) increased freshwater flux (i.e., precipitation minus evaporation, or $P-E$) in the Luzon Strait. Both mechanisms have the effect of decreasing sea surface salinity in the Luzon Strait, thus increasing the vertical gradient of salinity, and increasing stratification.

In addition to ENSO, the location of the Kuroshio modulates stratification in the Luzon Strait. During positive (negative) *N* anomalies, SSH is anomalously low (high) in the Luzon Strait, indicating the absence (presence) of a Kuroshio intrusion (Figure 4). However, NINO3.4 SST explains little of the variance in annual Luzon Strait SSH ($p > 0.05$, $r^2 < 0.02$), indicating that Kuroshio intrusions occur independently of ENSO, and that the positive *N* anomalies during La Niña are driven by a regional increase in $P-E$ rather than ENSO controlling the location of the Kuroshio.

The climate-driven changes in IW activity that we report are likely accompanied by other sources of variability. For example, in some cases, storms can increase IW energy flux via inertial-tidal interaction [*Hopkins et al.*, 2014]. Tidal forcing also influences IW generation and the energy associated with IWs in the NSCS [*Lien et al.*, 2005]. Cycles in tidal forcing, from fortnightly to interannual, are periodic by nature and will be superimposed upon the climate-driven trends in IW activity that we focus on here. To illustrate this, we plot temporal changes in tidal amplitude in the center of our Luzon Strait box following *Ray* [2013] (Figure 2 inset). Annual mean and maximum tidal amplitude vary ±5% mainly due to the 18.6 year lunar nodal cycle [*Pugh*, 1987], with no long-term trend.

4.3. Projections of Internal Wave Activity in the 21st Century

Our findings imply that changes in IW activity in the NSCS are driven by warming of the upper ~100 m of the ocean and modulated interannually by ENSO and Kuroshio intrusions. ENSO drives regional $P-E$, which combined with high-salinity Kuroshio intrusions into the Luzon Strait causes substantial interannual

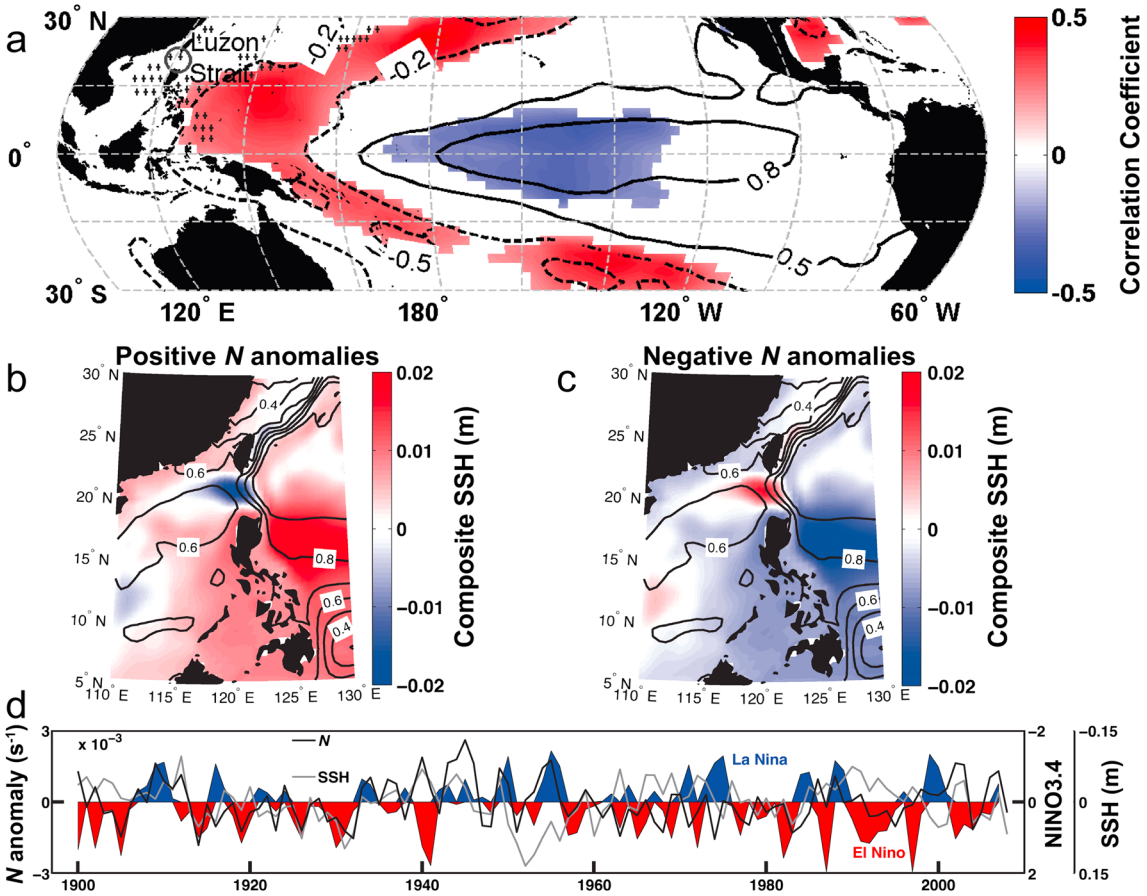

Figure 4. The roles of ENSO and the Kuroshio in driving interannual variability of stratification in the Luzon Strait. (a) Map of significant correlations between annual Luzon Strait *N* (colors) calculated with climatological mean temperature (only salinity varying) and ERSST.v3b [*Smith et al.*, 2008] for the period 1900–2008. Solid (dashed) black lines show contours of positive (negative) correlation coefficient (*r*) between ERSST.v3b and the NINO3.4 index, indicating the spatial pattern of ENSO. Speckling indicates significant positive correlations between annual Luzon Strait *N* calculated with climatological mean salinity (only temperature varying) and ERSST.v3b (no significant negative correlations). (b and c) Composite maps of detrended SSH anomalies during positive (Figure 4b) and negative (Figure 4c) annual Luzon Strait buoyancy frequency anomalies. Contours show the climatological mean SSH field, which clearly reveals the climatological position of the Kuroshio by the sharp horizontal SSH gradient just east of Luzon Strait in the Philippine Sea. Contour spacing is 0.1 m. (d) Time series of annual detrended Luzon Strait *N* (black), NINO3.4 index (red and blue), and SSH anomalies (gray). Note that NINO3.4 and SSH are plotted with reversed axes.

variability in Luzon Strait *N* (Figure 2). Future IW activity in the NSCS will therefore depend on how these drivers of stratification in the Luzon Strait respond to increasing radiative forcing in the 21st century.

To predict future change in NSCS IW activity, we calculated Luzon Strait *N* using the CCSM4 GCM. The historical (1900–2005) CCSM4 simulation produces a significant trend of increasing *N* of similar magnitude as SODA (Figure 2), demonstrating that the GCM accurately represents the response of Luzon Strait *N* to historical radiative forcing. Given confidence that CCSM4 can reliably simulate changes in Luzon Strait stratification in response to radiative forcing, we find that future Luzon Strait *N* is predicted by CCSM4 to increase steadily throughout the 21st century under medium (RCP4.5) and high (RCP8.5) greenhouse gas emission scenarios. These predicted stratification changes have several implications for the IW field in the NSCS. IWs will likely occur during a greater portion of the year as Luzon Strait stratification more frequently exceeds the critical level required to generate IWs. Further, the IWs are expected to become larger under greater stratification, increasing the flux of energy onto the NSCS continental shelf where these IWs elevate nutrient concentrations, enhance primary productivity, and potentially buffer coral reef ecosystems from the impacts of climate change.

5. Conclusions

Over the past century, IW activity in the NSCS has been modulated by climate-driven changes in water column stratification in the Luzon Strait and has increased in response to radiative forcing. Under future

warming, the NSCS will likely experience a more active IW climate and a seasonal expansion of the IW season toward winter. Future changes in stratification may affect the IW field globally, with important implications for other coastal ecosystems. Where the mechanisms of IW generation are similar to the NSCS, future changes in IW climate may represent an important, yet little recognized, aspect of the changes in the marine environment to which precious coastal ecosystems are exposed.

Acknowledgments

We thank Anne Cohen (WHOI) for insightful discussions and support of this study, Benjamin Giese (Texas A&M University), and Jim Carton (University of Maryland) for making SODA publicly available, the WHOI CMIP5 Community Storage Server for providing access to CCSM4 output (http://www.cesm.ucar.edu/models/ccsm4.0/), NCAR and all of the modeling groups associated with the Coupled Model Intercomparison Project phase 5 (CMIP5) effort, and Nick Tufillaro (Oregon State University) for pointing us to useful HICO images of internal waves in the NSCS. SODA and ERSST data were downloaded from the IRI/LDEO Climate Library (http://iridl.ldeo.columbia.edu). NINO3.4 data were downloaded from the University Corporation for Atmospheric Research (http://www.cgd.ucar.edu). Deployment of the temperature logger on Dongsha was possible because of generous support from Keryea Soong (National Sun Yat-sen University) and the Dongsha Atoll Marine National Park. This work was supported by NSF award 1220529 to Anne Cohen, by the Academia Sinica (Taiwan) through a thematic project grant to G.T.F.W. and Anne Cohen, by the Alfred P. Sloan Foundation and the WHOI Oceans and Climate Change Institute/Moltz Fellowship through awards to K.B.K., and by an NSF Graduate Research Fellowship to T.M.D. Temperature data from Dongsha Atoll and analysis codes are available upon request from T.M.D. (tdecarlo@whoi.edu). The authors thank three anonymous reviewers for their insightful comments.

The Editor thanks three anonymous reviewers for their assistance in evaluating this paper.

References

Baines, P. (1982), On internal tide generation models, *Deep Sea Res., Part A*, *29*(3), 307–338.

Carton, J. A., and B. S. Giese (2008), A reanalysis of ocean climate using Simple Ocean Data Assimilation (SODA), *Mon. Weather Rev.*, *136*(8), 2999–3017.

Chuang, W.-S., and D.-P. Wang (1981), Effects of density front on the generation and propagation of internal tides, *J. Phys. Oceanogr.*, *11*(10), 1357–1374.

Dai, C. (2004), Dong-sha Atoll in the South China Sea: Past, present and future, paper presented at Islands of the World VIII International Conference, Kinmen Island, Taiwan.

Drenkard, E., A. Cohen, D. McCorkle, S. de Putron, V. Starczak, and A. Zicht (2013), Calcification by juvenile corals under heterotrophy and elevated CO_2, *Coral Reefs*, *32*(3), 1–9.

Edmunds, P. J. (2011), Zooplanktivory ameliorates the effects of ocean acidification on the reef coral *Porites* spp, *Limnol. Oceanogr.*, *56*(6), 2402.

Fu, K. H., Y. H. Wang, L. St Laurent, H. Simmons, and D. P. Wang (2012), Shoaling of large-amplitude nonlinear internal waves at Dongsha Atoll in the northern South China Sea, *Cont. Shelf Res.*, *37*, 1–7.

Giese, B. S., and S. Ray (2011), El Niño variability in simple ocean data assimilation (SODA), 1871–2008, *J. Geophys. Res.*, *116*, C02024, doi:10.1029/2010JC006695.

Gregg, M. C., T. B. Sanford, and D. P. Winkel (2003), Reduced mixing from the breaking of internal waves in equatorial waters, *Nature*, *422*(6931), 513–515.

Holcomb, M., D. C. McCorkle, and A. L. Cohen (2010), Long-term effects of nutrient and CO_2 enrichment on the temperate coral *Astrangia poculata* (Ellis and Solander, 1786), *J. Exp. Mar. Biol. Ecol.*, *386*(1), 27–33.

Holligan, P., R. Pingree, and G. Mardell (1985), Oceanic solitons, nutrient pulses and phytoplankton growth, *Nature*, *314*(6009), 348–350.

Hopkins, J. E., G. R. Stephenson, J. A. M. Green, M. E. Inall, and M. R. Palmer (2014), Storms modify baroclinic energy fluxes in a seasonally stratified shelf sea: Inertial-tidal interaction, *J. Geophys. Res. Oceans*, *119*, 6863–6883, doi:10.1002/2014JC010011.

Lien, R.-C., T. Y. Tang, M. H. Chang, and E. A. D'Asaro (2005), Energy of nonlinear internal waves in the South China Sea, *Geophys. Res. Lett.*, *32*, L05615, doi:10.1029/2004GL022012.

Lin, I., W. T. Liu, C. C. Wu, G. T. Wong, C. Hu, Z. Chen, W. D. Liang, Y. Yang, and K. K. Liu (2003), New evidence for enhanced ocean primary production triggered by tropical cyclone, *Geophys. Res. Lett.*, *30*(13), 1718, doi:10.1029/2003GL017141.

Ma, B. B., R.-C. Lien, and D. S. Ko (2013), The variability of internal tides in the Northern South China Sea, *J. Oceanogr.*, *69*(5), 619–630.

McDougall, T. J. (2011), Getting started with TEOS-10 and the Gibbs Seawater (GSW) Oceanographic Toolbox.

Nash, J. D., S. M. Kelly, E. L. Shroyer, J. N. Moum, and T. F. Duda (2012a), The unpredictable nature of internal tides on continental shelves, *J. Phys. Oceanogr.*, *42*(11), 1981–2000.

Nash, J. D., E. L. Shroyer, S. M. Kelly, M. E. Inall, T. F. Duda, M. D. Levine, N. L. Jones, and R. C. Musgrave (2012b), Are any coastal internal tides predictable?, *Oceanography*, *25*(2), 80–95.

Pan, X., G. T. F. Wong, F. K. Shiah, and T. Y. Ho (2012), Enhancement of biological productivity by internal waves: Observations in the summertime in the northern South China Sea, *J. Oceanogr.*, *68*(3), 1–11.

Phillips, O. (1977), *The Dynamics of the Upper Ocean*, Cambridge Univ. Press, London.

Pugh, D. T. (1987), *Tides, Surges and Mean Sea-Level: A Handbook for Engineers and Scientists*, 472 pp., John Wiley, Chichester, U. K.

Ramp, S., Y. Yang, and F. Bahr (2010), Characterizing the nonlinear internal wave climate in the northeastern South China Sea, *Nonlinear Proc. Geophys.*, *17*(5), 481–498.

Ray, R. D. (2013), Precise comparisons of bottom-pressure and altimetric ocean tides, *J. Geophys. Res. Oceans*, *118*, 4570–4584.

Roder, C., L. Fillinger, C. Jantzen, G. M. Schmidt, S. Khokiattiwong, and C. Richter (2010), Trophic response of corals to large amplitude internal waves, *Mar. Ecol. Prog. Ser.*, *412*, 113–128.

Shaw, P. T., D. S. Ko, and S. Y. Chao (2009), Internal solitary waves induced by flow over a ridge: With applications to the northern South China Sea, *J. Geophys. Res.*, *114*, C02019, doi:10.1029/2008JC005007.

Smith, T. M., R. W. Reynolds, T. C. Peterson, and J. Lawrimore (2008), Improvements to NOAA's historical merged land-ocean surface temperature analysis (1880–2006), *J. Clim.*, *21*(10), 2283–2296.

Taylor, K. E., R. J. Stouffer, and G. A. Meehl (2012), An overview of CMIP5 and the experiment design, *Bull. Am. Meteorol. Soc.*, *93*(4), 485–498.

Torrence, C., and G. P. Compo (1998), A practical guide to wavelet analysis, *Bull. Am. Meteorol. Soc.*, *79*(1), 61–78.

Trenberth, K. E., and D. P. Stepaniak (2001), Indices of El Niño evolution, *J. Clim.*, *14*(8), 1697–1701.

Wall, M., L. Putchim, G. M. Schmidt, C. Jantzen, S. Khokiattiwong, and C. Richter (2015), Large-amplitude internal waves benefit corals during thermal stress, *Proc. R. Soc. B*, *282*, 20140650, doi:10.1098/rspb.2014.0650.

Wang, Y. H., C. F. Dai, and Y. Y. Chen (2007), Physical and ecological processes of internal waves on an isolated reef ecosystem in the South China Sea, *Geophys. Res. Lett.*, *34*, L18609, doi:10.1029/2007GL030658.

Wu, L., W. Cai, L. Zhang, H. Nakamura, A. Timmermann, T. Joyce, M. J. McPhaden, M. Alexander, B. Qiu, and M. Visbeck (2012), Enhanced warming over the global subtropical western boundary currents, *Nat. Clim. Change*, *2*(3), 161–166.

Yang, H., and L. Wu (2012), Trends of upper-layer circulation in the South China Sea during 1959–2008, *J. Geophys. Res.*, *117*, C08037, doi:10.1029/2012JC008068.

Zhang, Z., O. Fringer, and S. Ramp (2011), Three-dimensional, nonhydrostatic numerical simulation of nonlinear internal wave generation and propagation in the South China Sea, *J. Geophys. Res.*, *116*, C05022, doi:10.1029/2010JC006424.

Zhao, Z., and M. H. Alford (2006), Source and propagation of internal solitary waves in the northeastern South China Sea, *J. Geophys. Res.*, *111*, C11012, doi:10.1029/2006JC003644.

Zheng, Q., R. D. Susanto, C. R. Ho, Y. T. Song, and Q. Xu (2007), Statistical and dynamical analyses of generation mechanisms of solitary internal waves in the northern South China Sea, *J. Geophys. Res.*, *112*, C03021, doi:10.1029/2006JC003551.